

## Shock-induced reaction synthesis of cubic boron nitride

M. T. Beason,<sup>1</sup> J. M. Pauls,<sup>2</sup> I. E. Gunduz,<sup>1</sup> S. Rouvimov,<sup>3</sup> K. V. Manukyan,<sup>4</sup> K. Matouš,<sup>5</sup> S. F. Son,<sup>1,a)</sup> and A. Mukasyan<sup>2</sup>

<sup>1</sup>*School of Mechanical Engineering, Purdue University, West Lafayette, Indiana 47907, USA*

<sup>2</sup>*Department of Chemical and Biomolecular Engineering, University of Notre Dame, Notre Dame, Indiana 46556, USA*

<sup>3</sup>*Department of Electrical Engineering, University of Notre Dame, Notre Dame, Indiana 46556, USA*

<sup>4</sup>*Nuclear Science Laboratory, Department of Physics, University of Notre Dame, Notre Dame, Indiana 46556, USA*

<sup>5</sup>*Department of Aerospace and Mechanical Engineering, University of Notre Dame, Notre Dame, Indiana 46556, USA*

(Received 30 November 2017; accepted 3 April 2018; published online 24 April 2018)

Here, we report ultra-fast (0.1–5  $\mu$ s) shock-induced reactions in the 3B-TiN system, leading to the direct synthesis of cubic boron nitride, which is extremely rare in nature and is the second hardest material known. Composite powders were produced through high-energy ball milling to provide intimate mixing and subsequently shocked using an explosive charge. High-resolution transmission electron microscopy and X-ray diffraction confirm the formation of nanocrystalline grains of c-BN produced during the metathetical reaction between boron and titanium nitride. Our results illustrate the possibility of rapid reactions enabled by high-energy ball milling possibly occurring in the solid state on incredibly short timescales. This process may provide a route for the discovery and fabrication of advanced compounds. *Published by AIP Publishing.* <https://doi.org/10.1063/1.5017836>

A shockwave passing through a porous material results in a drastic increase in both pressure and temperature, which can induce solid-state polymorphic phase transformations<sup>1</sup> and shock-induced chemistry.<sup>2</sup> Detonation of a solid explosive is the most common example of shock induced chemistry, where a shock wave propagates at a steady velocity and reaction travelling a short distance behind the shock sustains the propagation through acoustic feedback from the gas phase products. This rapid reaction is typically only possible in gas producing systems of energetic compounds; however, there has long been interest in whether a reaction can occur within a shockwave for a condensed phase reaction and form useful solid products.<sup>2,3</sup>

Shock-induced reaction synthesis (SRS), which involves a combination of self-sustained, high-temperature (2000–3000 K) reactions and a shock wave, represents a unique method to produce advanced materials. SRS has been applied to many reactive systems, resulting in the synthesis of a significant number of solid compounds including carbides,<sup>3,4</sup> borides,<sup>5</sup> silicides,<sup>6</sup> and aluminides.<sup>7</sup>

However, fundamentally, there are two distinguishing cases for SRS.<sup>8</sup> In the first case, the shock wave heats the material enough that, after pressure release, the material reacts through a deflagration combustion wave with a characteristic reaction time on the order of several milliseconds. Numerous works have demonstrated the existence of such a route through recovery experiments, showing product formation after shock loading.<sup>9–13</sup> In the second case, a gasless reaction takes place directly in the shockwave within several microseconds.<sup>7,14</sup> In general, two methods have been suggested to prove the existence of such ultra-fast gasless reaction.<sup>15</sup> The more common approach involves an *in-situ* measurement and comparison of the shock Hugoniot for reactive and inert mixtures which

allows an inference of reaction occurring on the timescale of the shockwave.<sup>16–20</sup> The second approach is through the synthesis and recovery of a metastable phase, which can form only under high-pressure conditions. Throughout the history of SRS studies, this second approach has not been applied. The precise reaction conditions become even more intriguing for reactive systems with an adiabatic combustion temperature ( $T_{ad}$ ) below the melting points of all precursors, intermediates, and final products, a class of reactions known as the solid flame.<sup>21,22</sup> For such systems, solid-state mechanisms of mass transport are suspected to govern the reaction process. The boron (B)-titanium nitride (TiN) system, investigated in this work, leads to the formation of boron nitride (BN) and adheres to the prerequisites for the solid flame class of reactions.

The high pressure behavior of boron nitride (BN) has fascinated researchers since the middle of the last century.<sup>23,24</sup> Being the second hardest known material, cubic BN (c-BN) possesses superior chemical and thermal stabilities (stable up to 1650 K), as compared to diamond (stable up to 950 K),<sup>25</sup> is rarely found in nature,<sup>26</sup> and forms only under high-pressure and high-temperature (high P/T) conditions.<sup>23</sup> As a result, c-BN does not form below 6 GPa in quasistatic conditions<sup>27</sup> and is not expected below 12 GPa under shock loading.<sup>1</sup> It is important to note that a single shock loading of the hexagonal phase of BN (h-BN) results in a martensitic transformation to wurtzitic BN (w-BN) and not c-BN.<sup>28</sup> The thermal stability of c-BN makes it less susceptible to reversion to the graphitic form due to residual heat upon unloading as compared to diamond. This feature makes it a promising phase to use as an indicator to determine if reaction and product phase formation occur during the shock.

In this work, we provide direct evidence for the formation of c-BN as a result of shock-induced reactions using TiN as the nitrogen source for B. By this observation and

<sup>a)</sup>Author to whom correspondence should be addressed: sson@purdue.edu

taking into account that *c*-BN can be formed only at high *P/T*, we support the claim that under certain conditions, solid-state reactions (solid flame) may occur at ultra-fast rates in the time span range of 0.1–5  $\mu$ s.

The reactive mixture of B and TiN at a 3:1 molar ratio was selected to synthesize *c*-BN under shock loading. Thermodynamic calculations show that BN and titanium diboride (TiB<sub>2</sub>) are the equilibrium products for this exothermic reaction



The calculated  $T_{\text{ad}}$  for the system is 1903 K, which is lower than the melting points of B (2353 K), TiN (3203 K), and TiB<sub>2</sub> (3503 K), as well as the dissociation temperature of BN (3246 K). This suggests that the considered 3B + TiN mixture may behave as a solid flame system. Studies of this system have shown that, under locally initiated impulse heating, the reaction front exhibits oscillatory propagation, and the analysis of the product phase through XRD shows *h*-BN and TiB<sub>2</sub> to be the reaction products.<sup>29</sup>

It was previously shown that direct SRS of BN from a virgin mixture of commercially available micron size beta-rhombohedral ( $\beta$ -r) B and TiN powders is essentially impossible due to the high effective activation energy associated with mass diffusion kinetics for this solid-state reaction.<sup>29</sup> To overcome these difficulties, the reactivity was enhanced by the preparation of nanostructured composites through high-energy ball milling (HEBM) (see [supplementary material](#) for material preparation).

XRD performed on the powder produced by this intensive mechanical treatment [Fig. 1(a)] reveals only TiN and  $\beta$ -r B phases, indicating that no other crystalline phases formed during the HEBM process. Electron micrographs show that the produced powder consists of micron scale composite particles [Fig. 1(b)], which consist of nanoscale (5–500 nm) crystallites of B suspended in a fine (10–100 nm) TiN matrix [Fig. 1(c)]. These nanostructured B/TiN composite particles are highly reactive due to the significant increase in the interfacial contact area and reduced diffusion distance as a result of the milling process [Fig. 1(d)]. The parameters

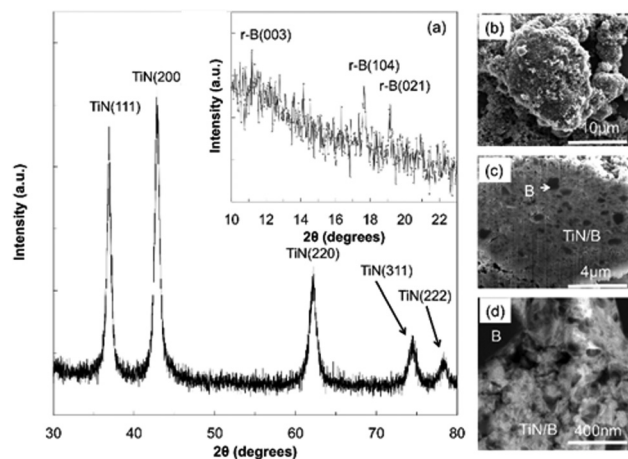


FIG. 1. XRD data (a) and micrographs (b)–(d) for the initial HEBM material. SEM and STEM images of a composite particle (b) and particle cross-sections (c) and (d) are shown in which the dark phase is B, while the lighter phase is TiN.

for the HEBM process and characteristics of initial reactants are listed in Table S1.

The reactive nanocomposite powder was loaded into a recovery capsule (Fig. S1) at a relative density in the range of 50%–55% and was shocked using approximately 25 g of PrimaSheet 1000 (a PETN based plastic explosive) to drive an outer copper shell at high velocities into a concentric copper tube that contained the powder. This method of powder compaction has been used in several configurations,<sup>30</sup> and the particular design used was modeled after Meyers and Wang.<sup>31</sup> The capsule was selected to sustain the high pressure from the shockwave for a longer duration as compared to direct contact with an explosive.<sup>31</sup> After compaction, the diameter of the shocked portion of the capsule remained constant along the entire length, suggesting that the sample was loaded evenly (Fig. S1). Simulations of the experiment were performed using a mixture equation of state developed using McQueen's mixture theory<sup>32</sup> from Hugoniot data for B<sup>33</sup> and TiN<sup>34</sup> in CTH<sup>35</sup> and are described in the [supplementary material](#).<sup>49,50</sup> The results indicate that the peak pressure achieved in the experiments is in the range of 15–20 GPa (Fig. S2). A release time constant ( $\tau$ ) is taken for a shock to transit the thickness of the flyer twice. For a shock velocity between 4 and 6 km/s and a 2 mm flyer thickness, the time constant would be  $\tau \sim 0.8$ –1.0  $\mu$ s. The pulse width  $\Delta t$  is estimated to be  $5\tau = 4$ –5  $\mu$ s. This result is in line with the 1–2  $\mu$ s pulse width observed in the simulations (Fig. S2).

Both XRD and SEM/TEM data confirm the formation of *c*-BN as a result of SRS. We examined the crystallographic parameters (d-spacing, Miller indices, reflection angles, and relative intensities) of the initial compounds ( $\beta$ -r B and TiN) and possible phases (TiB<sub>2</sub>, TiB, *h*-BN, and *c*-BN) resulting from the reaction (1) (Table S3). The detected strong TiB<sub>2</sub> peaks indicate that reaction occurred as a result of the shockwave. In addition to TiB<sub>2</sub> peaks, there are two peaks that can be attributed to the formation of BN phases, including *c*-BN [inset of Fig. 2(a)]. These peaks were found within samples taken from multiple cross-sections across several experiments at locations along the length of the recovery capsule,

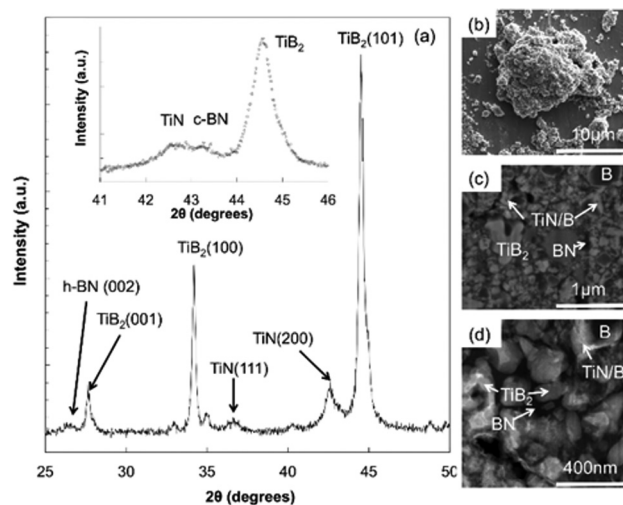


FIG. 2. XRD (a) and micrograph (b)–(d) data for the shocked materials. SEM and STEM images of a composite particle (b) and particle cross-sections (c) and (d) are shown in which the dark phase is BN with the lighter phase of TiB<sub>2</sub>, and some small regions consist of unreacted B surrounded by TiN.

indicating repeatable formation of c-BN. However, due to the low intensities of the BN peaks, further characterization was required to verify the formation of c-BN. It should be noted that the low intensities of B and BN peaks are associated with their low scattering factors and weight fractions as compared to the Ti-based phases and the small size of the synthesized crystals. As can be seen in the XRD of the initial material, despite the large volume fraction, the B peaks are substantially weaker than TiN peaks [Fig. 1(a)]. As a result, detailed structure and composition analyses of the materials were performed by electron microscopy based methods to verify the composition of the recovered material.

Figure 2 shows typical SEM (b and c) and STEM (d) images of a reacted particle. The particle has been cross-sectioned using the focused ion beam (FIB) slice and view technique to observe its structure in the reflection mode. Based on the SEM contrast, one can suggest the presence of four phases in the product material where light phases (B and BN) appeared with darker contrasts, while the phases with higher average atomic mass (e.g. TiN and TiB<sub>2</sub>) have lighter contrasts. EDS analysis with nm scale spatial resolution in the STEM mode (Fig. S4) confirmed the elemental composition of the phases (Table S4).

To analyze the morphology at the atomic level and crystal structure of the synthesized phases, high-resolution TEM (HRTEM) has been employed. Typical TEM images of a sample that has been subjected to the shock wave are shown in Fig. 3. The analysis of over ten regions, where complete reaction occurred, reveals that all consists of the three phases: TiB<sub>2</sub>, h-BN, and c-BN. The h-BN nanosheets are present in between the randomly oriented TiB<sub>2</sub> crystallites, while c-BN nanocrystals are primarily observed on the surface of the TiB<sub>2</sub> crystallites [see the inset in Figs. 3(a) and 3(b)].

During TEM imaging, the TiB<sub>2</sub> crystallite has been placed in a low index orientation, e.g., close to the  $\langle 001 \rangle$  zone. This low zone orientation has been critical for reliable identification of c-BN since other possible phases in the sample have d-spacings that are close (within 4%). HRTEM images have been used to identify the d-spacing with the required accuracy (down to 1%). It can be seen from Fig. 3(b) that 4-fold symmetry is recognizable.

It is known that the lattice parameters (d-spacing) of unstrained (perfect) crystals can be determined from HRTEM images with a relatively high accuracy of 0.2%.<sup>36</sup>

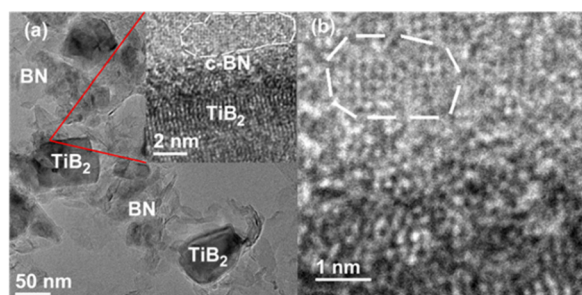


FIG. 3. (a) TEM images of typical particles formed in the Ti-B-N system after shock. Relatively large TiB<sub>2</sub> and h-BN crystallites are dominant within the field of view. The inset shows a magnified TEM image of the surface area of the large TiB<sub>2</sub> crystallite (70–100 nm in diameter) that has a thin layer of the c-BN phase. (b) Magnified area of the c-BN crystal phase at the interface with the TiB<sub>2</sub> crystalline particle.

The procedure typically involves the analysis of intensity profiles taken from HRTEM images of the crystal structures. However, the accuracy of this method decreases in the case of nanocrystals. Figure 4 shows an HRTEM image of a nanocrystal in a low zone crystallographic orientation. The averaged intensity profiles were used to measure the d-spacing in both horizontal and vertical directions to increase the signal-to-noise ratio. To exclude the systematic error associated with some minor variations in magnification, the magnification for a particular HRTEM image with one of the nanocrystals in question was corrected by the measurements of the d-spacings of known crystal structures. In this work, h-BN and/or TiB<sub>2</sub> were used as reference crystals to determine the correction factor. For example, the (0002) d-spacing of h-BN crystallites, measured on the same HRTEM image for calibration, appeared to be 0.345 ± 0.039 nm, instead of 0.333 nm (the database value), yielding a calibration factor of 0.96. The corrected d-spacing value for this nanocrystal was estimated to be 0.183 ± 0.014 nm, which fits within 1% accuracy of 0.181 nm, the (200) d-spacing of the c-BN crystal structure.

In order to provide further confirmation that the crystallites are the c-BN phase, we used JEMS<sup>37</sup> to simulate a HRTEM image and an atomic model of c-BN crystallites oriented in the  $\langle 001 \rangle$  zone [Fig. S5(a)]. The simulated atomic

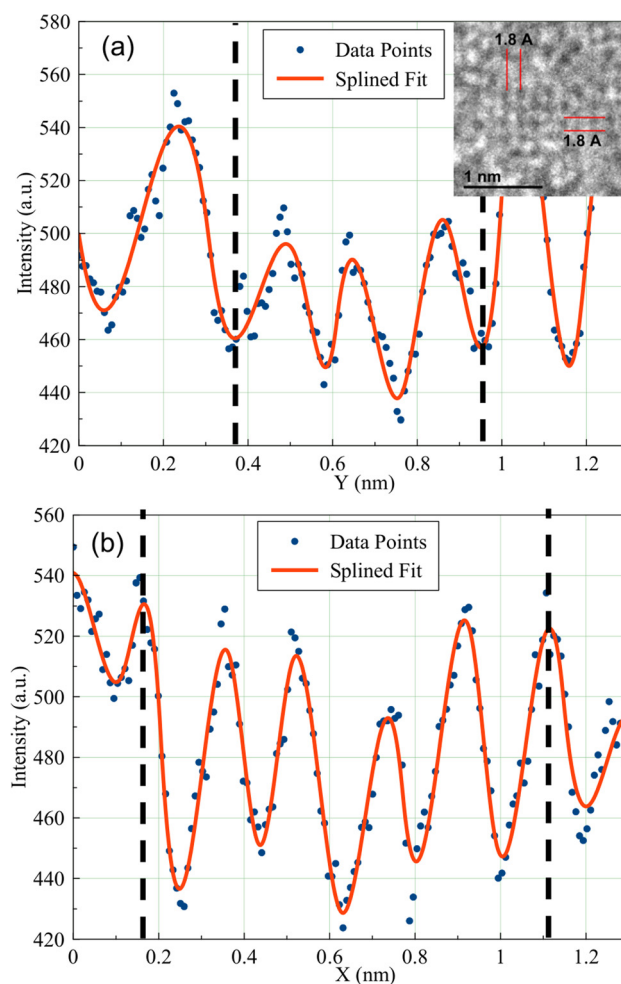


FIG. 4. Intensity distribution on the magnified fragment of the HRTEM image of the c-BN phase from Fig. 3 in vertical (a) and horizontal (b) directions showing that d-spacings in both directions are close to 0.18 nm.

columns of B atoms [Fig. S5(b)], which correspond to the white contrast on the HRTEM image taken at Scherzer focus [Fig. S5(c)], fit well with the c-BN structure.

Thus, it is clearly shown through XRD, HRTEM, and TEM modeling that c-BN has been formed through reaction between B and TiN after the shockwave (15–20 GPa) was applied to the initial reactive nanostructured media. Since the formation of c-BN requires high P/T, there is no doubt that we have observed shock-induced reaction, i.e. the products were formed in the time span of several  $\mu$ s. A thorough discussion of the expected temperature limits and their method of calculation is given in the [supplementary material](#) with the limiting behavior summarized here. The equilibrium shock temperature at pressure can be estimated by calculating the energy deposited through shock loading,  $\Delta e = 1/2 P\Delta V$ ,<sup>38</sup> and finding the temperature through integration of non-constant specific heats. Using data for  $\beta$ -B and TiN from the NIST Webbook,<sup>39</sup> the equilibrium shock temperature is found to be between 1600 and 2200 K. The lowest melting point in the B-TiN system is for B at 2350 K, which increases to approximately 2500 K at 20 GPa, as calculated using the Lindemann melting criteria.<sup>40,41</sup> This indicates that the shock temperature would be insufficient to melt B if the energy from compaction is evenly distributed throughout the sample. A high temperature limit would be if the energy is assumed to be localized to the material filling the pore-space, the rise in specific energy would double for the given input conditions. If the internal energy is localized in this fashion and the energy is partitioned between B and TiN based on their respective mass fractions,<sup>42</sup> which is justified by the intimate degree of mixing, approximately 18% of TiN would melt (assuming a non-pressure dependent melting point) with B remaining solid at a point frozen after an instantaneous shock rise. The temperature would then equilibrate to the value calculated above. However, the recovered powder, while having been fully compacted, maintained the overall morphology of the initial powder and specifically showed no indication of melt zones which has been shown to be evident of the metallographic analysis of shocked powders in several other works.<sup>43–45</sup> The analysis of the recovered powders is given in the [supplementary material](#) (Fig. S7). Furthermore, experiments performed on powder mixtures of 3B-TiN at identical initial densities showed that reaction did not occur (Fig. S3). If the temperatures were sufficient to melt B, significant reaction would be expected to take place.

Cylindrical shock loading is known to be conducive to shear instabilities in the deformed mixture,<sup>46</sup> and this may result in the formation of c-BN from h-BN due to localized shearing; however, since BN is not present in any form in the initial material (as determined through high resolution TEM and XRD), reaction would need to have already rapidly occurred for any polymorph of BN to be converted into c-BN. Any residual stress would not exceed the shear strength of TiN, which can be estimated for a perfect crystal of TiN from the shear modulus,  $G$ , of TiN as  $\tau_{\max} = G/30$ .<sup>47</sup> Taking an elastic modulus of 251 GPa<sup>48</sup> and estimating the Poisson ratio to be between 0.25 and 0.33, with  $G = E/2(1 + \nu)$ , the maximum shear strength in a perfect crystal of TiN is found to be between 3 and 3.3 GPa. This suggests that any residual stress would be below the necessary 6 GPa to drive formation

of c-BN, particularly considering that this would be the strength of a dislocation-free crystal. These results show that HEBM enables ultra-fast chemical reactions, which take place on the timescale of several microseconds, resulting in the formation of a high pressure polymorph (c-BN).

See [supplementary material](#) for additional experimental and computational methods.

The reported data are presented in the supplementary material. This work was supported by the Department of Energy, National Nuclear Security Administration, under the Award No. DE-NA0002377 as part of the Predictive Science Academic Alliance Program II. M. T. Beason was supported by the Department of Defense (DoD) through the National Defense Science and Engineering Graduate Fellowship (NDSEG) Program.

- <sup>1</sup>G. Duvall and R. Graham, *Rev. Mod. Phys.* **49**, 523 (1977).
- <sup>2</sup>D. E. Eakins and N. N. Thadhani, *Int. Mater. Rev.* **54**, 181 (2009).
- <sup>3</sup>N. N. Thadhani, *Prog. Mater. Sci.* **37**, 117 (1993).
- <sup>4</sup>W. Yang, G. M. Bond, H. Tan, T. J. Ahrens, and G. Liu, *J. Mater. Res.* **7**, 1501 (1992).
- <sup>5</sup>T. Kurita, H. Matsumoto, K. Sakamoto, T. Shimada, T. Osada, K. Ojima, and H. Abe, *J. Alloys Compd.* **396**, 133 (2005).
- <sup>6</sup>B. R. Krueger, A. H. Mutz, and T. Vreeland, *J. Appl. Phys.* **70**, 5362 (1991).
- <sup>7</sup>R. V. Reeves, A. S. Mukasyan, and S. F. Son, *Propellants, Explos. Pyrotech.* **38**, 611 (2013).
- <sup>8</sup>N. N. Thadhani, *J. Appl. Phys.* **76**, 2129 (1994).
- <sup>9</sup>R. V. Reeves, A. S. Mukasyan, and S. F. Son, *J. Phys. Chem. C* **114**, 14772 (2010).
- <sup>10</sup>B. A. Mason, L. J. Groven, and S. F. Son, *J. Appl. Phys.* **114**, 113501 (2013).
- <sup>11</sup>Y. Horie, R. A. Graham, and I. K. Simonsen, *Mater. Lett.* **3**, 354 (1985).
- <sup>12</sup>I. Song and N. Thadhani, *Metall. Mater. Trans. A* **23**, 41 (1992).
- <sup>13</sup>M. T. Beason, I. E. Gunduz, and S. F. Son, *Acta Mater.* **133**, 247 (2017).
- <sup>14</sup>D. Eakins and N. N. Thadhani, *J. Appl. Phys.* **100**, 113521 (2006).
- <sup>15</sup>A. N. Dremin and O. N. Breusov, *Russ. Chem. Rev.* **37**, 392 (1968).
- <sup>16</sup>S. S. Batsanov, G. S. Doronin, S. V. Klochkov, and A. I. Teut, *Combust. Explos. Shock Waves* **22**, 765 (1987).
- <sup>17</sup>D. L. Gur'ev, Y. A. Gordoplov, S. S. Batsanov, A. G. Merzhanov, and V. E. Fortov, *Appl. Phys. Lett.* **88**, 024102 (2006).
- <sup>18</sup>R. A. Graham, M. U. Anderson, Y. Horie, S. K. You, and G. T. Holman, *Shock Waves* **3**, 79 (1993).
- <sup>19</sup>X. Xu and N. N. Thadhani, *J. Appl. Phys.* **96**, 2000 (2004).
- <sup>20</sup>N. N. Thadhani, R. A. Graham, T. Royal, E. Dunbar, M. U. Anderson, and G. T. Holman, *J. Appl. Phys.* **82**, 1113 (1997).
- <sup>21</sup>A. G. Merzhanov, *Combust. Sci. Technol.* **98**, 307 (1994).
- <sup>22</sup>C. E. Shuck, K. V. Manukyan, S. Rouvimov, A. S. Rogachev, and A. S. Mukasyan, *Combust. Flame* **163**, 487 (2016).
- <sup>23</sup>R. H. Wentorf, Jr., *J. Chem. Phys.* **26**, 956 (1957).
- <sup>24</sup>S. S. Batsanov, G. E. Blokhina, and A. A. Deribas, *J. Struct. Chem.* **6**, 209 (1965).
- <sup>25</sup>V. L. Solozhenko and V. Z. Turkevich, *J. Therm. Anal.* **38**, 1181 (1992).
- <sup>26</sup>L. F. Dobrzhietskaya, R. Wirth, J. Yang, H. W. Green, I. D. Hutcheon, P. K. Weber, and E. S. Grew, *Am. Mineral.* **99**, 764 (2014).
- <sup>27</sup>L. Vel, G. Demazeau, and J. Etourneau, *Mater. Sci. Eng. B* **10**, 149 (1991).
- <sup>28</sup>T. Akashi, A. Sawaoka, S. Saito, and M. Araki, *Jpn. J. Appl. Phys., Part 1* **15**, 891 (1976).
- <sup>29</sup>T. S. Bilyan, K. V. Manukyan, S. L. Kharatyan, and J. A. Puszynski, *Int. J. Self-Propag. High-Temp. Synth.* **15**, 235 (2006).
- <sup>30</sup>J. W. Forbes, *Shock Wave Compression of Condensed Matter: A Primer*, 1st ed. (Springer-Verlag, Berlin, Heidelberg, 2012).
- <sup>31</sup>M. A. Meyers and S. L. Wang, *Acta Metall.* **36**, 925 (1988).
- <sup>32</sup>R. G. McQueen, S. P. Marsh, J. W. Taylor, J. N. Fritz, and W. J. Carter, *The Equation of State of Solids from Shock Wave Studies* (Academic Press New York, 1970).
- <sup>33</sup>S. P. Marsh, *LASL Shock Hugoniot Data* (University of California Press, 1980).

- <sup>34</sup>A. A. Bakanova, V. A. Bugayeva, I. P. Dudoladov, and R. F. Trunin, *Izv. Phys. Solid Earth C/C Fiz. Zemli Akad. Nauk* **31**, 513 (1995).
- <sup>35</sup>J. M. McGlaun and S. L. Thompson, *Int. J. Impact Eng.* **10**, 351 (1990).
- <sup>36</sup>J. Biskupek and U. Kaiser, *J. Electron Microsc. (Tokyo)*, **53**, 601 (2004).
- <sup>37</sup>P. Stadelmann, *JEMS Java Electron Microscopy Software* (2004), <http://cimewww.epfl.ch/people/Stadelmann/jemsWebSite/jems.html>.
- <sup>38</sup>L. Davison, *Fundamentals of Shock Wave Propagation in Solids* (Springer-Verlag, Berlin Heidelberg, 2008).
- <sup>39</sup>[NIST Chemistry WebBook: NIST Standard Reference Database Number 69](#), edited by P. J. Linstrom and W. G. Mallard (National Institute of Standards and Technology, Gaithersburg, MD, 2000), p. 20899.
- <sup>40</sup>S. Spiliopoulos and F. D. Stacey, *J. Geodyn.* **1**, 61 (1984).
- <sup>41</sup>M. Ross, *Phys. Rev.* **184**, 233 (1969).
- <sup>42</sup>V. F. Nesterenko, *Dynamics of Heterogeneous Materials* (Springer, New York, NY, 2001).
- <sup>43</sup>A. V. Molotkov, A. B. Notkin, D. V. Elagin, V. F. Nesterenko, and A. N. Lazaridi, *Fiz. Goreniya Vzryva* **27**, 117 (1991).
- <sup>44</sup>D. Raybould, *J. Mater. Sci.* **16**, 589–598 (1981).
- <sup>45</sup>W. Gourdin, *Prog. Mater. Sci.* **30**, 39 (1986).
- <sup>46</sup>V. F. Nesterenko, M. A. Meyers, H. C. Chen, and J. C. LaSalvia, *Appl. Phys. Lett.* **65**, 3069 (1994).
- <sup>47</sup>T. H. Courtney, *Mechanical Behavior of Materials* (Waveland Press, 2005).
- <sup>48</sup>H. O. Pierson, *Handbook of Refractory Carbides and Nitrides: Properties, Characteristics, Processing and Applications* (William Andrew, 1996).
- <sup>49</sup>D. E. Kittell, N. R. Cummock, and S. F. Son, “Reactive flow modeling of small scale detonation failure experiments for a baseline non-ideal explosive,” *J. Appl. Phys.* **120**, 064901 (2016).
- <sup>50</sup>D. J. Steinberg, S. G. Cochran, and M. W. Guinan, *J. Appl. Phys.* **51**(3), 1498 (1980).